Steglich, D.; Jeong, Y.; Andar, M.O.; Kuwabara, T..:
Biaxial Deformation Behaviour of AZ31 Magnesium Alloy: Crystal-Plasticity-Based Prediction and Experimental Validation
In: International Journal of Solids and Structures (2012) Elsevier

DOI: 10.1016/j.ijsolstr.2012.06.017

Biaxial Deformation Behaviour of AZ31 Magnesium Alloy: Crystal-Plasticity-Based Prediction and Experimental Validation

D. Steglich[a] , Y. Jeong[b], M. Andar[c], T. Kuwabara[d]

[a] Helmholtz-Zentrum Geesthacht Zentrum für Material- und Küstenforschung, Institute of Materials Research, Materials Mechanics, Max-Planck-Str. 1, 21502 Geesthacht, Germany

[b] Graduate Institute of Ferrous Technology, Pohang University of Science and Technology, San 31, Hyoja, Namgu, Pohang, Gyeongbuk, 790-784, South Korea

[c] Department of Mechanical Systems Engineering, Graduate School of Technology, Tokyo University of Agriculture and Technology, 2-24-16, Naka-cho, Koganei-shi, Tokyo, 184-8588, Japan

[d] Division of Advanced Mechanical Systems Engineering, Institute of Symbiotic Science and Technology, Graduate School of Tokyo University of Agriculture and Technology, 2-24-16, Nakacho, Koganei-shi, Tokyo, 184-8588, Japan

ABSTRACT – Plastic deformation of the commercial magnesium sheet alloy AZ31 under monotonous loadings has been investigated by means of mechanical tests and numerical simulations. Additionally to the commonly used uniaxial test two complementary mechanical tests have been performed: a biaxial test using cruciform specimens and a hydraulic bulge test. Both test lead to consistent results and evidence the differential strain hardening character of the considered material. A polycrystalline aggregate has been generated from measured texture data. Simulations using the visco-plastic self consistent (VPSC) scheme indicate the primary role of pyramidal slip in equibiaxial tension. Contours of equal plastic work have been generated using a methodology based on probing the aggregate in space of principal strains. The contours were compared with respective tests. Hardening parameters have been fitted in order to capture initial yield and evolution of iso-work contours. Limitations of the numerical framework's predictive capability as well as directions for parameter identification of phenomenological yield surfaces are formulated.

Key Words: Anisotropy, Plasticity, Plastic Work, VPSC, Biaxial Test, Differential Hardening

1 INTRODUCTION

Motivated by the growing demand for light weight materials, research on magnesium and its alloys has been getting more attention as magnesium is the lightest metal in use for the production of structural components in the automotive and aircraft industry. Despite the high strength-to-weight ratio, the application of wrought magnesium (i.e. sheets and extruded profiles) to light weight structures is limited. Existing applications are mainly based on cast products. The use of sheets for the fabrication of components and structures can still be expanded, taking advantage of cost-effective production of components by forming operations. The limitation for the structural application of magnesium sheets is correlated with its pronounced anisotropy, the tension-compression asymmetry as well as its comparably poor formability, especially at room temperature, see [1, 2]. A reason for this behaviour is the hexagonal-close packed (hcp) lattice structure which restricts the number of active deformation mechanisms in comparison to cubic metals. Therefore the ductility as well as the formability of magnesium sheets is limited, which partly restricts the whole process chain, i.e. the rolling procedures for magnesium sheets, the forming procedures of structural components and subsequently the mechanical properties of the resulting parts.

Recent research on magnesium branches into two main directions. The first is the development of new magnesium alloys with improved mechanical properties and especially improved formability, see e.g. [2]. The second topic deals with the effect of processing temperature, as a reasonable formability can be achieved at elevated temperatures, at which additional slip systems can be activated easily [3-5]. In any case, the application of wrought magnesium alloys requires reliable simulation tools for predicting the forming capabilities, the structural behaviour under mechanical loads and the lifetime of the component. The respective constitutive models have to account for the mentioned peculiarities of the mechanical behaviour, demanding for non state-of-the-art simulation techniques.

Crystal plasticity (CP) provides an appropriate tool for studying the mechanical phenomena on a micro-scale [6-10]. This approach requires detailed information on the local deformation mechanisms and the respective constitutive properties as well as on the distribution of crystallographic orientations of individual grains resulting from texture. Crystal plasticity is proven to be an adequate tool for understanding the micro-mechanisms of plastic deformations in hcp metals and for predicting their macroscopic properties [11]. However, for computation time considerations, it is obviously an improper approach to be applied for real-part forming simulations. The latter requires phenomenological modelling in the framework of continuum mechanics and the finite element (FE) method. Elasto-plastic or elasto-viscoplastic constitutive laws used for this purpose generally consist of a yield condition, a flow rule and a hardening

law. Depending on the considered material and the state variables involved, different yield conditions have been proposed, see [12, 13] for an overview. A yield condition usually involves a set of model parameters, which allow fitting the model predictions to mechanical tests in order to obtain a realistic description of the plastic behaviour. Here, strain hardening characteristic, anisotropy, time and temperature effects can be considered. It generally depends on the experimentalist's skills to separate these effects while performing a minimum amount of mechanical tests to determine the model parameters.

In current numerical analyses those yield surfaces are successfully used, which come along with a straightforward procedure to determine the built-in parameters. Because of its simplicity and its well-defined boundary conditions, the (uniaxial) tensile test conducted along different orientations is commonly considered as experimental input. The respective axial stress signal and the width reduction for each orientation provide two independent data. Beside uniaxial conditions, biaxial stress states should be included, because forming operations as well as service conditions generally involve multiaxial loadings. However, multiaxial loading experiments are difficult to perform and certainly are not without controversy in interpretation. Among the variety of tests described by Hecker [14], the hydraulic bulge test and the biaxial tension test using cruciform specimens have reached a high level of maturity [15]. These tests can best be employed for plane sheet metals considering radial loading paths in tension. They are frequently adopted to identify model parameters of the yield condition based on a certain value of deformation. Regarding modelling of hardening, the concept of isotropic hardening (yield surface expansion in stress space) dominates engineering practice. Other "elementary" hardening types can be distinguished, such as kinematic hardening (yield surface translation), rotational hardening (yield surface rotation) and distortional (or differential) hardening (shape change of the yield surface) [16]. Generally, hardening might be expressed by a combination of these elementary cases; experimental findings regarding distortional hardening have been reported by various authors e.g. by Hecker et al. [17], Hill et al. [18] and recently by Andar [19].

This paper studies plastic deformation of the well-established magnesium wrought alloy AZ31 (nominal composition of 3 wt.% Al, 1 wt.% Zn, 0.3 wt.% Mn, balance Mg) under static tensile loading conditions at room temperature and their prediction by numerical models. Beside the tensile test along the axes of orthotropy, two different testing procedures prescribing biaxial stress states are employed: biaxial tensile tests using cruciform specimen under various loading ratios and hydraulic bulge test. Respective simulations using the viscoplastic self-consistent (VPSC) scheme [10] are conducted and analysed in terms of contours of constant plastic work. The paper focuses on a micromechanical interpretation of the biaxial stress-strain curve, on rationalising the evolution of yield loci with increasing plastic strain and on providing directions for fitting of plane stress yield functions.

2 MAGNESIUM SHEET ALLOY AZ31

2.1 Characterisation

A commonly used magnesium alloy has been selected for the following investigations. AZ31 is commercially available and can be obtained from different suppliers. The rolled sheets used here have a thickness of 1mm. Tensile specimens (ASTM E8 sub size) used for the mechanical characterisation were cut by electro-discharge machining (EDM) to avoid the mechanical damage associated with conventional machining. Other specimens (cruciform and bulge) have been laser cut and shear cut, respectively, as in these cases the edge quality does not affect the measurements.

The microstructure of the investigated material can be inspected from **Figure 1**. It shows a fully recrystallised microstructure observed in the plane span by the rolling direction (RD) and the transverse direction (TD), (RD-ND)-plane. Regions with smaller grains are present in shear bands which developed during rolling. However, the grain size distribution can still be regarded as being homogenous. The average grain size measured in two perpendicular planes collinear with the normal direction (ND) is 5 microns.

The metallographic texture of the as-received material was quantified by means of X-ray diffraction using a Panalytical© texture goniometer. The samples for texture measurements were prepared from the middle sections of the sheets. Six incomplete pole figures were measured up to a tilt angle of 80°. From these data, the crystallographic orientation distribution (COD) was calculated. The re-calculated basal (0002) and prismatic (10-10) pole figures are shown in Figure 2. The AZ31 sheet has a strong basal texture with a preferential alignment of basal planes in the sheet plane (c-axis parallel to the normal direction (ND)). The frequently reported asymmetrical distribution of the basal texture components with respect to the ND on the (0002) pole [20-23], however, is not pronounced here. It is understood that this preferential alignment of the basal planes inhibits the accommodation of plastic deformation, because basal slip as the preferred deformation mechanism is not easily activated in such orientations [2, 24]. Thus, one may expect that deformation in the sheets thickness direction will be accommodated by a <c+a> slip mechanism or by twinning.

From the symmetry of the basal pole one can expect similar mechanical behaviour in tension along the rolling direction and along transverse direction. This is evidenced in **Figure 3**, which shows the tensile test responses of two representative tests, one conducted along the rolling direction, the other along the transverse direction. Stress signals as well as planar anisotropy (reduction of width) are similar in the considered loading cases. The fracture strain, however, differs significantly between the two orientations: the respective averages (6 specimens) are 0.21 for RD orientation and 0.15 for TD orientation.

2.2 Micromechanical modelling

Crystal plasticity models in general provide a means of relating the single crystal constitutive behaviour with that of the overall (polycrystalline) aggregate. They allow investigating the relationship of microstructural parameters like critical resolved shear stresses (CRSS) and texture on the macroscopic mechanical response. Two major classes of models share the same framework of describing slip along specific directions on well-defined planes on the level of a crystal: Finite Element (FE) based methods and so-called mean field models. While FE models fulfil local compatibility and equilibrium, and are therefore best suited for investigate grain interactions, polycrystal models assume that loading and deformation along the boundaries are uniform and that the volume average of stresses, strains and strain rates must coincide with respective quantities at the boundary. In order to fulfil this requirement, an assumption concerning the field quantities has to be made (e. g. Taylor, Sachs, self-consistency). For the numerical modelling work in this paper, a model based on the self-consistent scheme is used. It is briefly explained in the following.

Most modern polycrystal models invoke constitutive equation formulated on the level of the single crystal similar to the viscoplastic rule introduced by Asaro and Needleman [25], where the plastic strain rate $\dot{\boldsymbol{\varepsilon}}$ is related to the Cauchy stress tensor $\boldsymbol{\sigma}$ as follows:

$$\dot{\boldsymbol{\varepsilon}} = \dot{\gamma}_0 \sum_s \mathbf{m_s} \left(\frac{\mathbf{m_s} \cdot\cdot \boldsymbol{\sigma}}{\tau_s^c} \right)^n sgn\left(\mathbf{m_s} \cdot\cdot \boldsymbol{\sigma} \right). \tag{1}$$

$\dot{\gamma}_0$ is the effective shear step size, $\mathbf{m_s}$ are the Schmid tensors that resolve the grain level stress $\boldsymbol{\sigma}$ and strain rate $\dot{\boldsymbol{\varepsilon}}$ on to the slip systems s and *sgn* denotes the direction of the resolved stress. *n* is the rate sensitivity exponent, which is usually fixed at *n*=20 for all slip and twinning modes in order to mimic a rate-insensitive plastic behaviour while maintaining the advantages of a viscoplastic formulation for improved numerical convergence. The threshold stresses τ_s^c represent the stress required to activate the s^{th} slip (or twin) system. It can be constant during plastic deformation, or following an extended Voce hardening rule

$$\tau_s^c = \tau_s^0 + \left(\tau_s^1 + \theta_1 \gamma \right) \left[1 - \exp\left(-\frac{\theta_0 \gamma}{\tau_s^1} \right) \right] \tag{2}$$

as a function of accumulated shear strain, γ. τ_s^0 and τ_s^1 are the initial and back-extrapolated increase in the threshold stress, while θ_0 and θ_1 are the initial and final slope of the hardening curve, respectively. These four parameters per deformation mode constitute the hardening characteristics of the respective slip or twinning system. Additionally, it is generally important

to account for self and latent hardening for each deformation mode using a hardening matrix, which relates the effect of the s^{th} mode on the hardening of the t^{th} mode. This increase in the threshold stress of a system due to interaction is accounted for by means of a coupling parameter h^{st}. It empirically accounts for the obstacles that dislocations in slip system "t" represent for the activity of system "s". If there are k crystallographically equivalent slip/twinning modes and the i^{th} mode has n_i slip/twinning systems, h^{st} is assumed to have the following form [26]:

$$h^{st} = \begin{pmatrix} \mathbf{A}_{n_1 \times n_1} & q_{12}\mathbf{A}_{n_2 \times n_2} & \cdots & q_{1k}\mathbf{A}_{n_1 \times n_k} \\ q_{21}\mathbf{A}_{n_2 \times n_1} & \mathbf{A}_{n_2 \times n_2} & \cdots & q_{2k}\mathbf{A}_{n_2 \times n_k} \\ \vdots & \vdots & & \vdots \\ q_{k1}\mathbf{A}_{n_k \times n_1} & q_{k2}\mathbf{A}_{n_k \times n_2} & \cdots & \mathbf{A}_{n_k \times n_k} \end{pmatrix}. \tag{3}$$

$\mathbf{A}_{n_i \times n_j}$ is a $(n_i \times n_j)$-matrix completely populated by ones; q_{ij} represents the ratio of the latent hardening rate of mode j to the self-hardening rate of mode i. The increment in threshold stress is given by

$$\Delta\tau_s = \frac{d\tau_s^c}{d\gamma}\sum_t h^{st}\Delta\gamma^t, \tag{4}$$

with $\Delta\gamma^t$ as the shear accommodated by deformation mode "t" and

$$\gamma = \sum_\alpha \int \left|\dot{\gamma}^\alpha\right| dt \tag{5}$$

as the accumulated shear strain in the grain.

During the deformation of metals the contribution from elasticity is small compared to the plastic component. In addition, once the elasto-plastic transition is over, the evolution of stress in the grains is controlled by slip. As a consequence, elasticity is disregarded and only the plastic contribution to deformation is described. For obtaining a macroscopic ("averaged" or "effective") plastic mechanical response for the aggregate material, a coupling of the single crystal constitutive rule, Eq. (1), to the aggregate response has to be accomplished. In this study, this is done by using a self-consistent algorithm based upon the Eshelby inclusion formalism. During each straining increment, the grain level stresses and strain rates are solved to simultaneously satisfy Eq. (1), as well as the self-consistency criteria, i.e., the averages of all the grain level stresses and strain rates equal the boundary conditions imposed upon the aggregate. After each straining step, the grain strengths and crystallographic orientations (i.e., texture) are updated. The method is usually referred to as the "viscoplastic self-consistent scheme", VPSC. The details of this viscoplastic self-consistent polycrystal model and its numerical realisation can be found in [10, 27].

To apply the inclusion formalism it is necessary to linearise the nonlinear response. Several different methods, so-called self consistent schemes, have been proposed. Among them are the secant, the tangent, the affine and the effective interaction scheme. For an overview on the linearisation procedures the reader is referred to Lebensohn et al. [28]. While keeping texture and hardening parameters unchanged, each linearisation scheme predicts a different mechanical response. The parameters of a crystal plasticity model are then not "material parameters" in a rigorous sense. Thus it is necessary to interpret all model parameters together with the respective underlying scheme. For an assessment of the different methods to AZ31 the reader is referred to Wang et al. [29]. In what follows, the effective interaction scheme (n_{eff}=10) is used.

Various contributions have demonstrated the successful use of the VPSC approach for the prediction of texture evolution [8, 30], as well as of plastic yielding in (hcp) metals [31]. Recent applications of the VPSC formalism for the analysis of magnesium alloys include tension and compression of extruded rods [21], tension and in-plane compression of sheets [32], simple shear and torsion [26], in-plane and through-thickness compression [23], and even sophisticated forming operations [33-35]. An interesting overview of the different CP parameters used in the respective analyses can be found in [36].

Rolled magnesium alloy sheets typically display strong in-plane tension–compression asymmetry, i.e., the material yields at a significantly lower stress in compression than in tension [37]. This behaviour has been attributed to the mechanical twinning on the $\{10\bar{1}2\}$ planes in the $\langle 10\bar{1}1\rangle$ directions during compression but not during tension. This is due to the basal textures present in the investigated AZ31 sheets and the polar nature of twinning [38]. The twinning mechanism is accounted for by a family of pseudo-slip systems on the $\{10\bar{1}2\}$ plane in $\langle 10\bar{1}1\rangle$ direction and the Predominant Twin Reorientation Scheme (PTR) [10]: In case of c-axis tension, the system becomes active and a certain fraction of twinned volume is reoriented. In the investigations presented here the twinning plays only a secondary role, as in the first quadrant of the plane stress space twinning in rolled sheets is unlikely. However, the mechanism is included for the sake of completeness.

Table 1 lists the families of slip systems which are commonly used to describe deformation of magnesium alloys: 3 independent basal <a>, 3 prismatic <a>, 6 pyramidal <c+a> and 6 <c+a> systems describing twinning. For the description of the system's strength evolution, parameters reported in [26, 29] were adopted. They result from a careful assessment of the magnesium alloy AZ31 B (3.17 mm thickness). The authors examined the mechanical response in terms of stress and deformation behaviour in different directions and additionally considered the evolution of distinct texture components. Although the present material shows different deformation behaviour, some analogies are apparent. It is assumed that the calibrated micromechanical parameters can be used to numerically study general trends in yield surface evolution. Table 2 summarises the parameters associated with the hardening law, eq. (2).

The determination of self- and latent hardening parameters is not straight forward, and several parameter sets (to a certain extent contradictory) exist to model the mechanical behaviour of Mg-alloys. This – in general – questions the uniqueness of micromechanical parameters, as their choice strongly depends on the (macroscopic) target function, texture input and user preferences. With the considered systems, the interaction matrix, eq. (3), becomes a 24*24 matrix. The parameters q_{ij}, so-called latent hardening parameters, have been identified for the previously mentioned material and assumed to be $q_{14}= q_{24}= q_{44}=4$, $q_{34}=2$ [23, 26, 29, 33]. The values of q_{41}, q_{42}, q_{43} turn out to be irrelevant, because the twinning (the 4th family of systems) is assumed not to harden.

3 CONTOURS OF EQUAL PLASTIC WORK

The diffuse transition from the elastic to the plastic regime observed in many metals makes the definition of yielding problematic when considering different (multiaxial) stress states. For anisotropic metals, where the principal axes of stress and strain are generally not coincident, there are further complications in the choice of a suitable proof stress condition. A common way to circumvent these shortcomings is the use of the specific plastic work (plastic work per volume) to characterise yielding and strain hardening of polycrystals [39, 40]. These values might be more suitable and more descriptive for the average material's response over a wide deformation range. Therefore, in what follows, experimental and numerical results are compared by means of the specific plastic work

$$W_p = \int \boldsymbol{\sigma} \cdot\cdot d\boldsymbol{\varepsilon}^{pl}, \tag{6}$$

which can be easily computed from the plastic strain and stress response along any loading path. **Figure 4** illustrates the concept for the numerical analysis of a biaxially loaded three-dimensional polycrystalline aggregate:

- The aggregate is loaded monotonically under various pre-defined strain ratios ε_1: ε_2=2:-1; 4:-1; 1:0; 4:1; …
- In a post-processing step, for each loading path the plastic work W_p is calculated;
- For pre-defined discrete values of W_p the two in-plane stress components σ_1 and σ_2 are calculated by linear interpolation;
- The duple (σ_1, σ_2) constitutes a point on the respective iso-work contour in the space of principal stresses.

The values chosen for plastic work depend on the purpose of the characterisation. A common choice is to use values which correlate with certain pre-defined values of plastic strain in uniaxial tension along a reference direction (mostly the rolling direction) see e. g. [41]. Values of specific work close to zero allow for a definition of the (initial) yield surface, higher values characterise the hardening behaviour of the material. It is worth to note that the procedure described here does not prescribe radial stress paths in a rigorous way. A ratio of principal strain rates is given instead. The principal stress ratio can only be checked in retrospect, while the shear stresses as well as the out-of-plane normal stress are forced to be zero.

4 MECHANICAL BEHAVIOUR OF SINGLE CRYSTALS UNDER BIAXIAL LOADING CONDITIONS

The method is demonstrated in the following by three separate analyses of differently oriented single crystals. The orientations chosen are $\{0001\}$||ND, $\{2\bar{1}\bar{1}0\}$||RD (ND orientation), $\{10\bar{1}0\}$||ND, $\{0001\}$||RD (RD orientation) and $\{10\bar{1}0\}$||ND, $\{2\bar{1}\bar{1}0\}$||RD (TD orientation), see **Figure 5**. Principal strain rate components are prescribed along the boundaries of the effective aggregate, which here consists of one single grain. The resulting stress response is shown in terms of projections of the three-dimensional stress space to the plane stress space (σ_{RD}, σ_{TD}). The crystal plasticity parameters are taken from [29] and shown in table 2. In order to show the evolution of iso-work contours, three different values of the specific plastic work have been chosen: W_p=0.1 MPa (representing the initial yield surface), W_p=5 MPa and 20 MPa for an intermediate and high plastic deformation, respectively. The results are shown in **Figure 6**. The ND-orientation covers some aspects of the behaviour of a rolled sheet, as the alignment of the basal planes is similar to the main orientation in the sheet. Yielding in tension is predicted at higher stresses than in compression for small and intermediate values of plastic work. During compression along the principal stress directions twinning is activated. Due to the low CRSS of twinning this activation appears early, resulting in yielding at low stresses. However, after the reorientation after twinning, the highest value of plastic strain can only be accommodated by pyramidal and prismatic slip, which is hard to activate. This causes the pathological shape and the non-convexity of the highest iso-contour in **Figure 6**a. In case of equi-biaxial tension, the intermediate and the highest iso-work contour coincide. This is a consequence of the hardening law, Eq. (2), which predicts saturation of the stresses at higher shear strains. Thus, plastic work increases at constant stress by accumulation of plastic strain.

The mechanical behaviour of the crystal in RD- and TD-orientation shows similar characteristics, see **Figure 6**b and c. Certain combinations of orientation and loading direction allow for twinning, which results in a low yield stress followed by a sharp increase of the stress

after reorientation of the grain. All contours are angular, which is attributed to the binary character of the problem: most of the loading scenarios activate only one slip system. In the three cases shown, the basal system has a low Schmid factor and thus is not activated.

5 EXPERIMENTAL PROCEDURE

In order to obtain a realistic input for constitutive equations and to characterise the anisotropic plastic behaviour under biaxial stress states more sophisticated experimental tests than the uniaxial tensile test are required. Multiaxial loading experiments are rather complex and certainly not without controversy in interpretation. To study material response, the stress state needs to be determinant and homogeneous, which has restricted most investigations to thin sheet specimens loaded biaxially in plane stress or to thin-walled tubes loaded in combined axial load and torsion or axial load and internal pressure. The material under consideration is a plane sheet, thus direct tests have to be based on flat specimens. Among the set of possible experiments, two tests are considered in the following which address biaxial tensile loading using cruciform specimens and equi-biaxial loading as a special case of biaxial tension using hydraulic bulge tests. These tests are complementary in the sense that they are valid in different strain intervals: The results obtained from cruciform specimens are applicable for small strains (and therefore small values of plastic work), hydraulic bulge testing is usually performed to obtain a stress-strain relationship at strains beyond the fracture strain.

5.1 Biaxial Tensile Tests using cruciform Specimens

Biaxial tensile tests were carried out using the cruciform specimen proposed by Kuwabara et al. [42]. The geometry of the cruciform specimen used in this study is shown in **Figure 7**a. It is the same as used in [42, 43]. According to results of finite element analyses of the cruciform specimen with the strain measurement position depicted in **Figure 7**a, the error of stress measurement is estimated to be less than 2% [44]. For the details of the servo-controlled biaxial tensile testing machine used in this study, see [43]. The test setup allows imposing a biaxial stress state to the material while keeping the ratio of stresses in two orthogonal directions constant. Each cruciform specimen was subjected to proportional loading with nominal stress ratios $\sigma_{\mathrm{RD}} : \sigma_{\mathrm{TD}} = 4{:}1$, 2:1, 4:3, 1:1, 3:4, 1:2 and 1:4. Among the various ratios tested $\sigma_{\mathrm{RD}} : \sigma_{\mathrm{TD}} = 1{:}1$ refers to the equi-biaxial loading. The mechanical response in each test consists of two "independent" signals, stress-strain $\sigma_{\mathrm{RD}}(\varepsilon_{\mathrm{RD}})$ in rolling direction and stress-strain $\sigma_{\mathrm{TD}}(\varepsilon_{\mathrm{TD}})$, see Figure 8a for a special case of equi-biaxial test. Normal strain components $(\varepsilon_{RD}, \varepsilon_{TD})$ were measured using uniaxial strain gauges (YFLA-2, Tokyo Sokki Kenkyujo Co.) mounted at ±18 mm from center along the maximum loading direction. For details of the biaxial testing apparatus and testing method, refer to [43].

The concept of plastic work contour was adopted to determine the yield locus and subsequent work hardening characteristics of the test material. The stress-strain curve obtained from a uniaxial tensile test in RD was chosen as a reference datum for work hardening; the uniaxial true stresses σ_0 in RD, and the plastic work per unit volume, W_0, corresponding to particular values of offset logarithmic plastic strains $\varepsilon_0^{\mathrm{p}}$ were determined. The uniaxial true stresses σ_{90} in TD and the biaxial true stress components $(\sigma_{\mathrm{RD}}, \sigma_{\mathrm{TD}})$ were then determined at the same plastic work as W_0. The stress points $(\sigma_0,\ 0)$, $(0,\ \sigma_{90})$ and $(\sigma_{\mathrm{RD}}, \sigma_{\mathrm{TD}})$ thus plotted in the principal stress space comprise a plastic work contour corresponding to a particular value of $\varepsilon_0^{\mathrm{p}}$. When $\varepsilon_0^{\mathrm{p}}$ is taken as sufficiently small, the corresponding work contour can practically be viewed as a yield locus.

Two independent tests on cruciform specimens have been conducted under a prescribed stress ratio of 1:1. One of the test results is shown in **Figure 7**b in terms of total strain and true stress components. At a total strain of approx. 0.012, the specimen's arms have been torn apart, hence the test stopped. For comparison, the true stress – logarithmic strain curve obtained from uniaxial tests is included in **Figure 7**b. The increased tangent modulus in case of the biaxial stresses is clearly visible.

5.2 Hydraulic Bulge Tests

Measuring the biaxial stress-strain behaviour is possible by bulging a plane sheet by oil pressure and monitoring the bulge radius at the pole and the pressure [45]. The major limitation of this test is its constraint to a specific stress state by the geometry of the bulged specimen (a function of the shape of the die opening). Here, an Erichsen bulge/FLC tester (model 161) was used to perform the tests on AZ31 sheets using a circular die. When bulging the sheet, the pole of the bulge is stretched by a biaxial tension stress σ_b. Considering that through thickness stress is negligible, the in-plane principal stresses of the pole area are $\sigma_1 = \sigma_2 = \sigma_b$. Following the membrane theory, the biaxial stress is a function of the current radius of curvature R, the thickness t and the pressure p,

$$\sigma_b = \frac{pR}{2t}. \tag{7}$$

The current thickness t can be calculated from the initial thickness t_0 and the thickness strain ε_t,

$$t = t_0 \exp\left(-\varepsilon_t\right). \tag{8}$$

Assuming plastic isotropy of the material, the principal strains at the pole of the bulge are $\varepsilon_1=\varepsilon_2=\varepsilon_b$ (membrane strain), and $\varepsilon_{3=}\varepsilon_t$ (thickness strain). Considering that the material is incompressible during plastic deformation, the thickness strain is given by $\varepsilon_t=-2\,\varepsilon_b$.

The curvature radius *R* has been acquired using a mechanical device, similar to that proposed by Young et al. [45]. It consists of a tripod unit, see **Figure 8**a, a lever and a counter-weight (not shown in the figure). An extensometer and a LVDT (Linear Variable Differential Transformer) installed inside of the tripod system measure an in-plane elongation and the height difference between two fixed points on the bulge pole. From these data the biaxial strain and the radius of curvature, *R*, is determined. These quantities hence determine the biaxial stress, σ_b, via equations (8) and (7). For details on the systems design and its validation the reader is referred to [46].

Two successful quasistatic tests on AZ31 sheets at room temperature have been conducted until failure of the specimens appeared at the pole. **Figure 8**b shows dependency of the calculated membrane stress on the plastic contribution of the half thickness strain. The data show a large scatter resulting from a noisy pressure signal and the uncertainties of the curvature measurement at the onset of bulging. The maximum total plastic strain achieved is about 0.03, which is significantly higher than the maximum strain accomplished during tensioning the cruciform specimens.

For small strains the data obtained from the bulge tests may not be resilient, as the curvature of the sheet is almost infinite and hence the determination of the membrane stress following equation (7) is uncertain. However, in the range of plastic strain below 0.008 the bulge tests give the same results than the equibiaxial test obtained form the cruciform specimen. This gives cause to hope that both tests together yield a valid biaxial stress-strain curve, each test using its particular strength. The trend already visible through the data taken form the cruciform specimen is confirmed: The slope of the biaxial stress-strain curve is significantly higher than the uniaxial one, which confirms the differential hardening effect in AZ31 under monotonous tensile loadings.

6 VPSC SIMULATION RESULTS OF TEXTURED POLYCRYSTALS

Simulations of the mechanical behaviour were conducted on aggregates including 1000 discrete orientations representative of the initial texture. The discrete orientations were chosen to represent the measured texture as depicted in **Figure 2** following a procedure described by Toth and Houtte [47]. Positive normal strain rates are prescribed at the boundaries of the aggregate; shear strain rates are enforced to be zero. The shear stresses evolve with increasing deformation and have been controlled a posteriori to be small compared to the normal stresses. This investigation is restricted to strain paths leading to positive principal stresses, though only the

first quadrant in plane principal stress space is covered. More than 100 radial loading paths have been used to generate the figures shown in the following. First, the initial yield surface was generated by probing the aggregate. This initial yield surface is determined solely by the critical resolved shear stresses and the aggregate's initial texture. The subsequent contours of equal plastic work have been generated using the numerical procedure described in the previous section.

6.1 Established CP parameters

The VPSC-simulations are first conducted using the parameters of single crystals calibrated by Wang and Wu [19], see Table 2, and compared with the experimentally obtained data for plastic work contour levels of W_p=0.147 MPa, 0.337 MPa, 0.743 MPa, 1.181 MPa and 1.628 MPa, which correspond to irreversible uniaxial strains of 0.001, 0.002, 0.004, 0.006 and 0.008. The stresses are normalised by the respective yield stress in RD tension. The respective contours are shown in Figure 9. Some features of the predicted contours are described in the following. The first level usually can be regarded as the onset of yielding, but here a difference between predicted onset of yielding (PCYS in **Figure 9**) and the first iso-work contour is obvious. In particular in the biaxial stress state both curves differ. The initial yield surface shape appears compressed along the biaxial tension direction. The simulated biaxial yield stress is generally less then the measured one. With increasing deformation the contours of equal work get more bulged, similar to what has been observed in the experiments. However, the amount of bulging, which evidences the distortional character of hardening, is underestimated. The uniaxial responses in RD and TD are almost identical, which is due to the symmetric texture input. The elevated stress level in TD cannot be mapped to its full extent.

6.2 Updated CP parameters

In an attempt to better understand the macroscopic experimental observations – in particular the respective contributions of the active slip systems to the overall deformation – the critical resolved shear stresses (CRSS, τ_s^0) of the basal, prismatic and <c+a> pyramidal slip systems and their respective hardening have been reassessed. Deformation twinning, although considered in the modelling for the sake of completeness, is not relevant here. This mechanism is only active in c-axis tension, and from the texture information it is clear that in the first quadrant of the principal stress space this mechanism remains inactive.

The first contour of equal plastic work, W_p=0.147 MPa, was used to calibrate the CRSS of the three slip systems. Based on the assumption that the ratios of the CRSS influence the shape of the initial yield locus for a given texture, the ratios have been varied to fit the inner shape while simultaneously meeting the yield point in uniaxial (RD) tension, see **Figure 10**. In a second step the hardening parameters τ_s^1, θ_1 and θ_2 are calibrated to meet both, the contours of equal plastic

work and the biaxial stress-strain curve, see **Figure 8**b. The resulting parameters are summarised in table 3. While a perfect fit could be obtained in case of the two inner contours, the outer contours agree with the experiments well in the biaxial regime, but they overestimate the response in case of uniaxial tension (intersections of the contours with the x-axis). This effect is present in the simulations depicted in **Figure 9** as well, but not visible due to the normalisation. Therefore, for a quantitative assessment, **Figure 10** and **Figure 11** use the non-normalised values of the recorded stresses. **Figure 11** confirms what is indirectly visible in **Figure 10**: both tensile tests are well captured by the simulation for very small strains, but for strains larger than 0.005 the uniaxial response is overestimated by the simulation. During the fitting procedure it was possible only to fit one of the tests with a set of parameters correctly. The "crossing" between the two curves is managed via a shift of the strength ratio between prismatic and pyramidal slip, compare table 3. Although better agreement could not be achieved, the results elucidate the fact that the r-value, the ratio of plastic contributions of thickness and width strain during tensile testing, is not constant but increases with increasing strain. At the beginning of deformation the plastic thickness strain is much smaller than the plastic width strain, which leads to an r-value close to zero. This is in line with the slope of the initial yield surface, which intersects the x-axis almost perpendicular and experimental findings generated from repeated loading-unloading of a tensile specimen and measurement of the irreversible strain components [19]. Note that the ratio of plastic strains is used to calculate the r-value in **Figure 12**a, instead of the ratio of total strains.

One advantage of CP models in general is the possibility to monitor the contribution of each slip system to the overall deformation behaviour. This is usually done by providing the relative activity of a family of systems *s*, which describes the contribution of a specific deformation mode to the total plastic strain increment. It is calculated with respect to the increase of deformation,

$$\text{activity}_s = \frac{\Delta\gamma_s}{\sum_s \Delta\gamma_s}, \tag{9}$$

providing information on the actual contribution of the respective mechanism. An explanation of the different hardening behaviour in uniaxial and biaxial tension is given in **Figure 12**b. It shows the relative activities of each family of slip systems calculated with the VPSC simulation. In uniaxial tension basal slip is active throughout the deformation process. Pyramidal and prismatic swap their dominance: While prismatic slip becomes active, pyramidal activity becomes less pronounced. This is to some extent reversed in case of biaxial tension. Prismatic slip is not active at all; the deformation has to be compensated primarily by basal and pyramidal slip. This is in agreement with the findings of Hama and Takuda [48] based on an artificially created rolling texture, who explain the flattening of the initial work contour with the dominant basal slip activity. The pyramidal system is activated early in case of biaxial loading, and hence

accommodated deformation which can be compensated by prismatic slip in case of uniaxial tension because of its higher Schmid factor. Since the hardening in pyramidal slip is highest this leads to the bulging of the iso-work contours in the vicinity of biaxial stress states. Note that the twinning activity in case of biaxial tension is almost zero, while it is significantly higher in case of uniaxial tension. Although the texture is a basal one, a few grains are oriented in a way which allows c-axis tension. Considering the fact that the CRSS for twinning is lower than the basal CRSS (see [36] for a summary), those grains will immediately be activated by twinning. Hence the hardening parameters of twinning have an influence on the initial yield surface: in particular the intersection angle with the axes is affected, which in turn determines the r-value.

7 DISCUSSION AND CONCLUSION

The VPSC framework has been shown to be a powerful tool to predict texture evolution and macroscopic plastic properties of polycrystalline aggregates. In the investigations presented here one important input is missing: In the considered (small) stain regime texture evolution does not take place. Respective scans of the bulged sample revealed no change of the initial texture. Hence the available input is limited to the mechanical tests. It is shown here that the observed effects can be explained to a certain extent by adjusting the sensitivity of the four basic deformation systems. A deduction in a rigorous sense is certainly delicate and not foreseen by the authors. While the effect of the grain number used in the modelling of the polycrystal could be eliminated by a convergence study, the effect of the linearisation scheme used is ubiquitous. As already mentioned earlier, the parameters of a crystal plasticity model are then not “material parameters” in its classical meaning. Thus it is necessary interpret all model parameters together with the respective underlying scheme. In this context it is worth to remember that latent hardening, eqs. (3) and (4), is considered only for the twinning system: slip system interaction is assumed not to take place, while slip system hardening will affect twinning system hardening: $q_{14}= q_{24}= q_{44}=4$, $q_{34}=2$. Once these parameters will be changed, the complete identification process has to be repeated (except for the initial yield surface).

Biaxial stretching is the dominant deformation mode in sheet metal forming. Thus, it is necessary that the plasticity model used for a forming prediction accurately describes this stress state. The equibiaxial yield stress is an important quantity characterising the shape of the yield surface. It can be determined by means of the bulge test or by means of an equibiaxial tensile test. An alternative method is to conduct a through-thickness compression test, as the uniaxial compression test causes the same deviatoric stress state as an equibiaxial tensile test, thereby being equivalent to the latter one. The through-thickness compression test suffers from the (undetermined) effect of friction, thus the determination of the stress response is delicate. Furthermore, it is may be questionable, particular in case of hcp materials, if yielding is independent of the hydrostatic pressure, see e. g. [39]. Respective disk-compression experiments conducted in the context of this work with identical material revealed a stress level being 10%

higher than the one obtained from bulge and biaxial tensile test – and therefore are not included here. One may circumvent the problem related to the stress signal in general by using a purely geometric quantity like the biaxial r-value, which provides information concerning the slope of the tangent to the yield surface in the equibiaxial stress point. This method, however, is restricted to fitting an initial yield surface and does not allow for a characterisation of material hardening.

The hydraulic bulge test, initially designed to benefit from the delayed necking of the specimens compared to uniaxial testing, has an additional advantage: Once the (membrane) stress can be determined, it generates valuable information about the yield surface evolution. Doubts may be justified with respect to the underlying assumptions, which allow the calculation of the membrane stress: transversal isotropy of the material and no variation of the stress through the sheet's thickness. Whereas the latter can be controlled by the ratio of bulge diameter and sheet thickness, the hypothesis of isotropy is certainly violated. Aretz and Keller [49] recently showed by numerical analyses, that for biaxial r-values equal to one the stress-strain curve obtained from the bulge test consistently describes the biaxial hardening behaviour. The anisotropy along the orthotropic axes alone is not harmful. The biaxial test results reported here suggest that this criterion ($r_b \approx 1$) is fulfilled, thus the bulge test is valid. Unfortunately, the test design leads to an early failure of the specimen if the material shows little strain hardening like the one considered here. Fortunately, the bulge test can bridge this deficit. This gives cause to hope that both tests together yield a valid biaxial stress-strain curve, each test exploiting its particular strength: the cruciform specimens provide accurate stress-strain data below failure of the respective specimen; the bulge test covers the regime of higher strains best.

Concerning the significance of initial yield for a yield surface determination this study clearly reveals that either the sharp changes of the contours of equal plastic work have to be modelled by means of distorsional plasticity. Alternatively, once a simpler model is preferred, the calibration process should be conducted using an intermediate value of plastic work. The prediction capability of any phenomenological plasticity model depends not only on the accuracy of its initial yield locus. For structural assessment, for example, a deformation process over a large strain interval has to be predicted correctly. In the field of metal forming, or once ductile damage phenomena are considered, this becomes essential. The investigations presented here exemplify that initial yield and subsequent yield surfaces may appear significantly different. Beside the frequently reported anisotropy in magnesium alloys it shows a pronounced differential hardening effect. While using a plastic potential appropriate for deformation of hcp materials (e. g. [50, 51]) combined with isotropic hardening – which is a common choice in engineering – one should fit the parameters of the potential over a wide range of strains instead of considering the point of initial yield only. The example presented here shows that the latter might be misleading.

ACKNOWLEDGEMENTS

The present work was conducted during a sabbatical leave of D.S. at the Graduate Institute of Ferrous Technology (G.I.F.T.) of POSTECH, Pohang, South Korea as part of an international outgoing fellowship (Marie Curie Actions) of the 7th programme of the European Commission. The authors acknowledge this support and hereby point out that the EU is not responsible for the content of this paper. The authors furthermore thank R. Lebensohn and C. Tomé for providing the VPSC code and POSCO for providing the sheet material. The fruitful discussions with S. Agnew and T. Hama as well as the assistance of L. Xu and J. Lee during the experiments are appreciated.

LITERATURE

[1] Hosford WF. The mechanics of crystals and textured polycrystals. New York: Oxford University Press, 1993.
[2] Bohlen J, Nuernberg MR, Senn JW, Letzig D, Agnew SR. The texture and anisotropy of magnesium–zinc–rare earth alloy sheets. Acta Mater. 2007;55:2101-2112.
[3] Dröder KG. Untersuchungen zum Umformen von Feinblechen aus Magnesiumknetlegierungen. Maschinenbau. Hannover: Universität Hannover; 1999.
[4] Avedesian MM, Baker H, editors. Magnesium and Magnesium Alloys: ASM International; 1999.
[5] Agnew SR, Duygulu Ö. A Mechanistic Understanding of the Formability of Magnesium: Examining the Role of Temperature on the Deformation Mechanisms. Materials Science Forum. 2003;419 - 422:177-188.
[6] Peirce D, Asaro RJ, Needleman A. Material rate dependence and localized deformation in ductile single crystals. Acta Metall. 1983;31(12):1051-1076.
[7] Peirce D, Asaro RJ, Needleman A. Material rate dependence and localized deformation in crystalline solids. Acta Metall. 1983;31(12):1951-1976.
[8] Lebensohn RA, Tomé CN. A self-consistent viscoplastic model: prediction of rolling textures of anisotropic polycrystals. Materials Science and Engineering: A. 1994;175(1-2):71-82.
[9] Staroselsky A, Anand L. A constitutive model for hcp materials deforming by slip and twinning: application to magnesium alloy AZ31B. International Journal of Plasticity. 2003;19(10):1843-1864.
[10] Lebensohn RA, Tomé CN. A self-consistent anisotropic approach for the simulation of plastic deformation and texture development of polycrystals: application to zirconium alloys. Acta Metallurgica et Materialia. 1993;41:2611-2624.
[11] Graff S, Brocks W, Steglich D. Yielding of magnesium: From single crystal to polycrystalline aggregates. Int J Plast. 2007;23(12):1957-1978.
[12] Barlat F. Constitutive Descriptions For Metal Forming Simulations. Numiform'07. Porto: American Institute of Physics; 2007.

[13] Barlat F, Cazacu O, Zyczkowski M, Banabic D, Yoon JW. Yield Surface Plasticity and Anisotropy. In: Raabe D, Roters F, Barlat F, Cheng L-Q, editors. Continuum Scale Simulation of Engineering Materials. Weinheim: Wiley-VCH, 2004. p. 146-183.
[14] Hecker S. Experimental studies of yield phenomena in biaxially loaded metals. Annual meeting of the American Society of Mechanical Engineers. New York, NY, USA: ASME; 1976.
[15] Kuwabara T. Advances in experiments on metal sheets and tubes in support of constitutive modeling and forming simulations. International Journal of Plasticity. 2007;23(3):385-419.
[16] Aretz H. A simple isotropic-distortional hardening model and its application in elastic-plastic analysis of localized necking in orthotropic sheet metals. International Journal of Plasticity. 2008;24(9):1457-1480.
[17] Stout MG, Hecker SS, Bourcier R. An evaluation of anisotropic effective stress-strain criteria for the biaxial yield and flow of 2024 aluminum tubes. Journal of Engineering Materials and Technology. 1983;105(4):242-249.
[18] Hill R, Hecker SS, Stout MG. An investigation of plastic flow and differential work hardening in orthotropic brass tubes under fluid pressure and axial load. International Journal of Solids and Structures. 1994;31(21):2999-3021.
[19] Andar O, Steglich D, Kuwabara T. Measurement and Analysis of the Biaxial Loading and Unloading Behavior of AZ31 Mg Alloy Sheet. In: Chinesta F, Chastel Y, El Mansori M, editors. International Conference on Advances in Materials and Processing Technologies (AMPT2010). Paris, France: AIP; 2010. p. 75-80.
[20] Kaiser F, Letzig D, Bohlen J, Styczynski A, Hartig C, Kainer KU. Anisotropic properties of magnesium sheet AZ31. Materials Science Forum. 2003;419-422:315-320.
[21] Ebeling T, Hartig C, Laser T, Bormann R. Material law parameter determination of magnesium alloys. Materials Science and Engineering: A. 2009;527(1-2):272-280.
[22] Agnew SR, Duygulu Ö. Plastic anisotropy and the role of non-basal slip in magnesium alloy AZ31B. Int J Plast. 2005;21(6):1161-1193.
[23] Jain A, Agnew SR. Modeling the temperature dependent effect of twinning on the behavior of magnesium alloy AZ31B sheet. Materials Science and Engineering: A. 2007;462(1-2):29-36.
[24] Wonsiewicz BC, Backofen WA. Plasticity of magnesium crystals. Trans Metall Soc AIME. 1967;239:1422-1433.
[25] Asaro RJ, Needleman A. Texture development and strain hardening in rate dependent polycrystals. Acta Metall. 1985;33(6):923-953.
[26] Wang H, Wu Y, Wu PD, Neale KW. Numerical Analysis of Large Strain Simple Shear and Fixed-End Torsion of HCP Polycrystals. Cmc-Computers Materials & Continua. 2010;19(3):255-284.
[27] Tomé CN, Lebensohn RA. Manual for Code VISCO-PLASTIC SELF-CONSISTENT (VPSC) (Version 7c). Los Alamos National Laboratory, USA; 2009.
[28] Lebensohn RA, Tome CN, Castaneda PP. Self-consistent modelling of the mechanical behaviour of viscoplastic polycrystals incorporating intragranular field fluctuations. Philosophical Magazine. 2007;87(28):4287-4322.
[29] Wang H, Raeisinia B, Wu PD, Agnew SR, Tomé CN. Evaluation of self-consistent polycrystal plasticity models for magnesium alloy AZ31B sheet. International Journal of Solids and Structures. 2010;47(21):2905-2917.

[30] Lebensohn RA, Canova GR. A self-consistent approach for modelling texture development of two-phase polycrystals: application to titanium alloys. Acta Mater. 1997;45(9):3687-3694.
[31] Plunkett B, Lebensohn RA, Cazacu O, Barlat F. Anisotropic yield function of hexagonal materials taking into account texture development and anisotropic hardening. Acta Mater. 2006;54(16):4159-4169.
[32] Choi SH, Kim DH, Lee HW, Seong BS, Piao K, Wagoner R. Evolution of the deformation texture and yield locus shape in an AZ31 Mg alloy sheet under uniaxial loading. Materials Science and Engineering A. 2009;526(1-2):38-49.
[33] Neil JC, Agnew SR. Crystal plasticity-based forming limit prediction for non-cubic metals: Application to Mg alloy AZ31B. International Journal of Plasticity. 2009;25:379–398.
[34] Beausir B, Suwas S, Tóth LS, Neale KW, Fundenberger J-J. Analysis of texture evolution in magnesium during equal channel angular extrusion. Acta Materialia. 2008;56(2):200-214.
[35] Walde T, Riedel H. Modeling texture evolution during hot rolling of magnesium alloy AZ31. Materials Science and Engineering: A. 2007;443(1-2):277-284.
[36] Lou XY, Li M, Boger RK, Agnew SR, Wagoner RH. Hardening evolution of AZ31B Mg sheet. International Journal of Plasticity. 2007;23(1):44-86.
[37] Kelley EW, Hosford WF. The deformation characteristics of textured magnesium. Trans Metall Soc AIME. 1968;242:654-661.
[38] Yoo MH. Slip, twinning, and fracture in hexagonal close-packed metals. Metall Trans A. 1981;12A:409-418.
[39] Lowden MAW, Hutchinson WB. Texture strengthening and strength differential in Titanium-6AL-4V. Metallurgical Transactions. 1975;A 6(3):441-448.
[40] Hill R, Hutchinson JW. differential hardening in sheet-metal under biaxial loading - A theoretical framework Journal of Applied Mechanics. 1992;59(2):S1-S9.
[41] Kuwabara T, Kuroda M, Tvergaard V, Nomura K. Use of abrupt strain path change for determining subsequent yield surface: experimental study with metal sheets. Acta Materialia. 2000;48(9):2071-2079.
[42] Kuwabara T, Van Bael A, Lizuka E. Measurement and analysis of yield locus and work hardening characteristics of steel sheets wtih different r-values. Acta Materialia. 2002;50(14):3717-3729.
[43] Kuwabara T, Ikeda S, Kuroda K. Measurement and analysis of differential work hardening in cold-rolled steel sheet under biaxial tension. Journal of Materials Processing Technology. 1998;80-81(0):517-523.
[44] Hanabusa Y, Takizawa H, Kuwabara T. Evaluation of accuracy of stress measurements determined in biaxial stress tests with cruciform specimen using numerical method. Steel Research International. 2010;81(Supplement Metal Forming 2010):1376-1379.
[45] Young RF, Bird JE, Duncan JL. An automated hydraulic bulge tester. Journal of Applied Metalworking. 1981;2(1):11-18.
[46] Xu L. Constitutive Modeling of High Strength Steel Sheets. Department of Ferrous Technology, Graduate Institute of Ferrous Technology. Pohang: University of Science and Technology; 2011. p. 154.
[47] Toth LS, Houtte P. Discretization Techniques for Orientation Distribution Functions. Texture and Microstructures. 1992;19:229-244.

[48] Hama T, Takuda H. Crystal plasticity finite-element simulation of work-hardening behavior in a magnesium alloy sheet under biaxial tension. Computational Materials Science. 2012;51(1):156-164.
[49] Aretz H, Keller S. On the non-balanced biaxial stress state in bulge-testing. Steel Research int, special edition. 2011;Material Characterization and Modelling:738-743.
[50] Plunkett B, Cazacu O, Barlat F. Orthotropic yield criteria for description of the anisotropy in tension and compression of sheet metals. International Journal of Plasticity. 2008;24(5):847-866.
[51] Steglich D, Brocks W, Bohlen J, Barlat F. Modelling direction-dependent hardening in magnesium sheet forming simulations. International Journal of Material Forming. 2011;4(2):243-253.

Table 1: Deformation modes considered in the present work

Name	Number of Slip Systems	Plane	Slip Direction
Basal $\langle \mathbf{a} \rangle$	3	$\{0001\}$	$\langle 11\bar{2}0 \rangle$
Prismatic $\langle \mathbf{a} \rangle$	3	$\{\bar{1}100\}$	$\langle 11\bar{2}0 \rangle$
Pyramidal $\langle \mathbf{a}+\mathbf{c} \rangle$	6	$\{11\bar{2}2\}$	$\langle 11\bar{2}3 \rangle$
Tensile Twin	6	$\{10\bar{1}2\}$	$\langle 10\bar{1}1 \rangle$

Table 2: Direct hardening parameters following [29], Eq. (2)

	basal $\langle \mathbf{a} \rangle$	prismatic $\langle \mathbf{a} \rangle$	pyramidal $\langle \mathbf{a}+\mathbf{c} \rangle$	tensile twinning
τ_s^0	17	77	148	33
τ_s^1	6	33	35	0
θ_0	3800	650	9600	0
θ_1	100	50	0	0

Table 3: Calibrated direct hardening parameters, Eq. (2)

	basal $\langle \mathbf{a} \rangle$	prismatic $\langle \mathbf{a} \rangle$	pyramidal $\langle \mathbf{a}+\mathbf{c} \rangle$	tensile twinning
τ_s^0	28	110	96	2
τ_s^1	15	100	50	30
θ_0	8000	600	6000	6000
θ_1	500	400	500	0

Figures

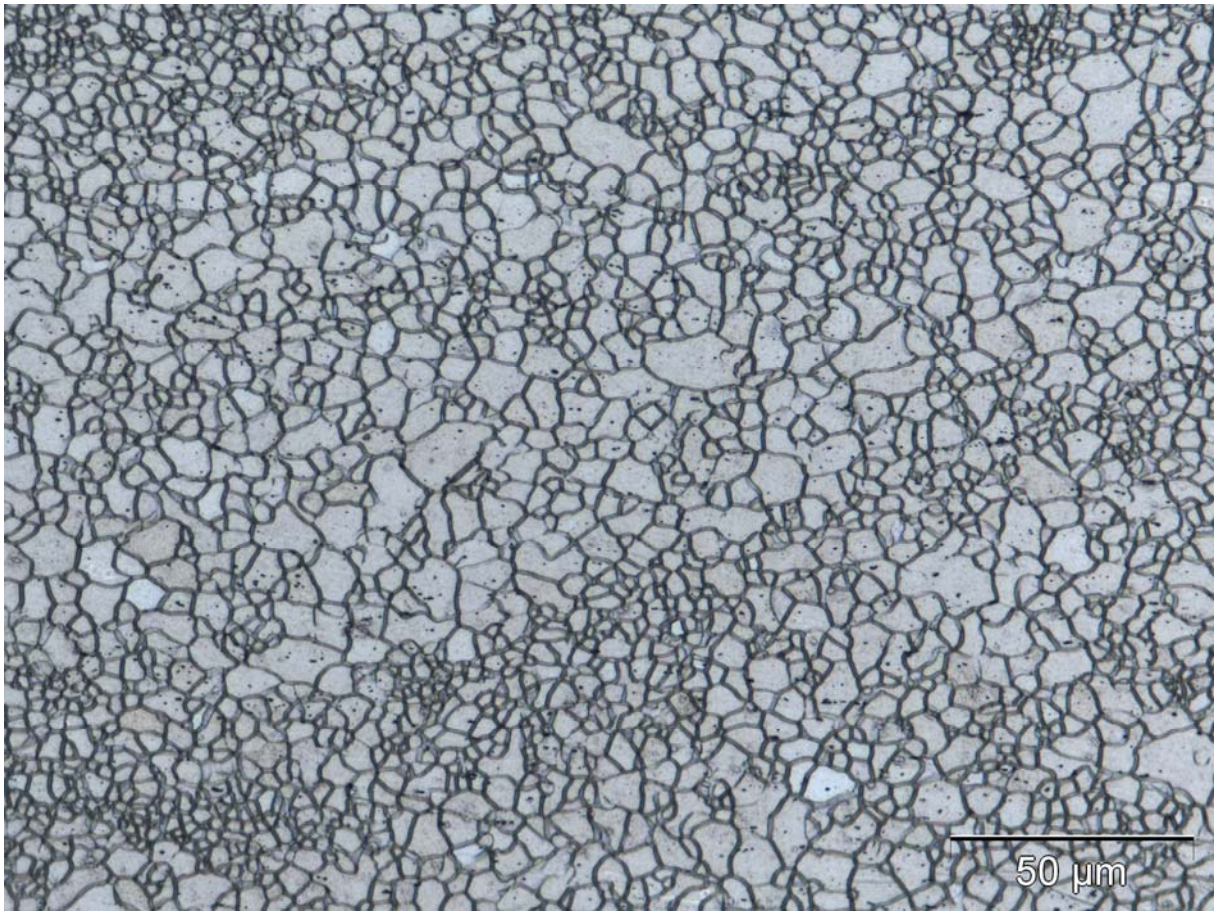

Figure 1: Micrograph of a longitudinal section (RD-ND plane) of the AZ31-sheet showing a recrystallised microstructure

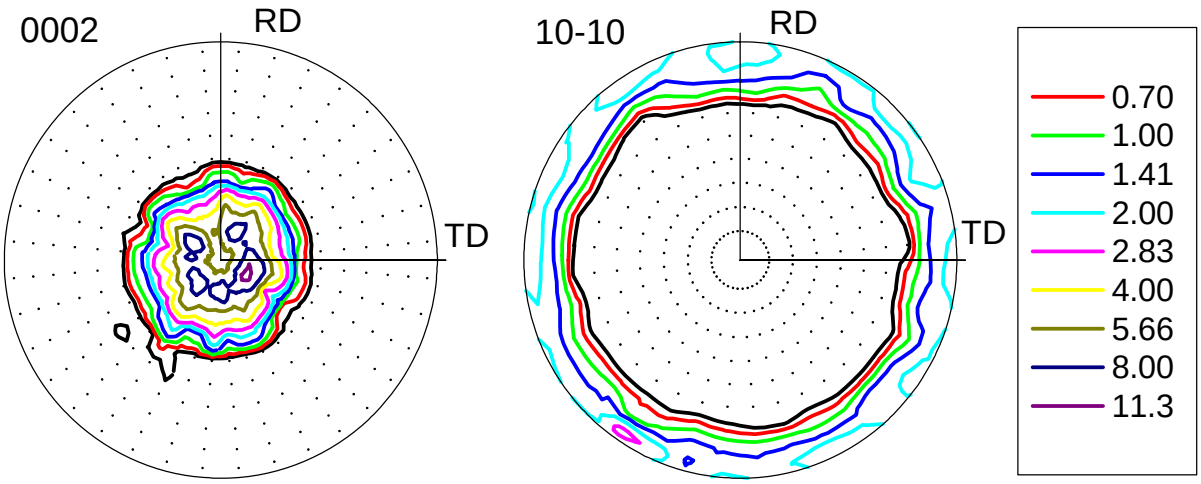

Figure 2: Basal (0002) and prismatic (10-10) pole figures of the AZ31-sheet

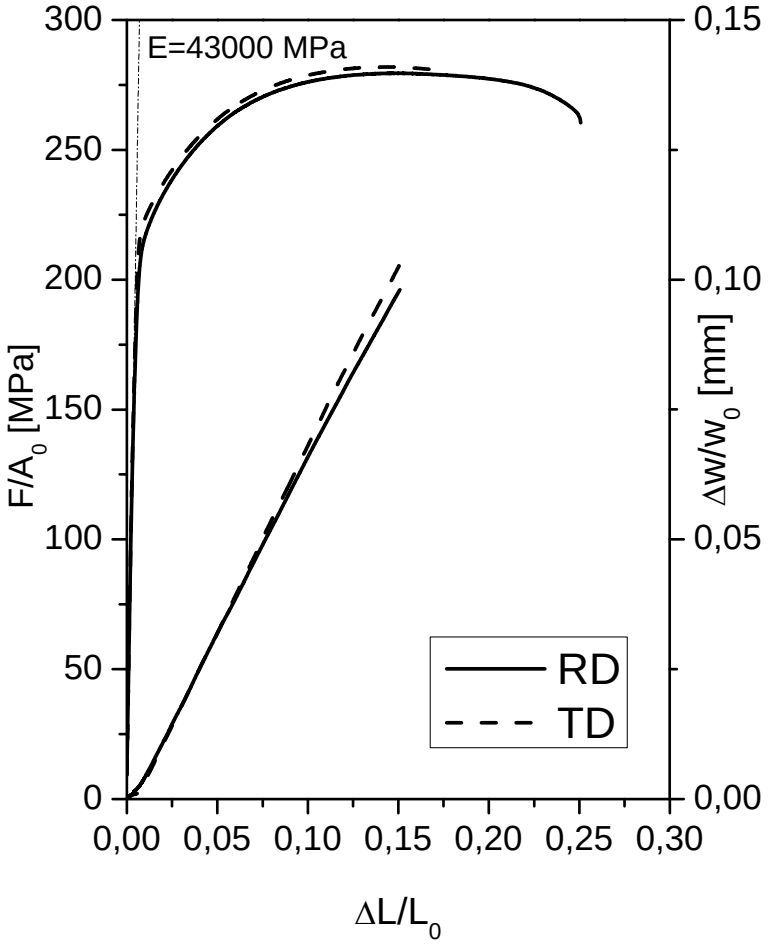

Figure 3: Results of two representative tensile tests: along rolling direction (RD) and along transverse direction (TD)

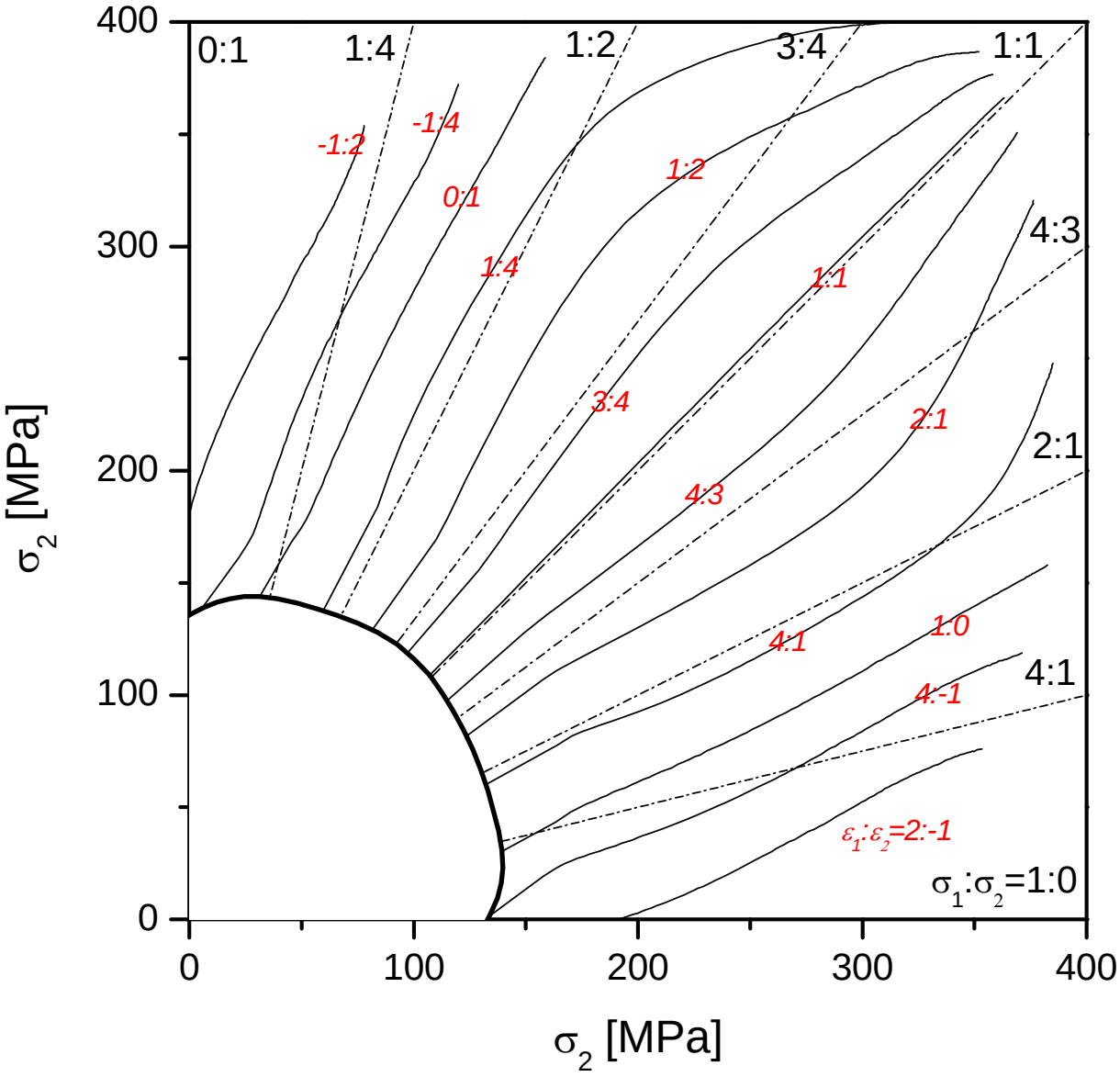

Figure 4: Construction of contours of equal plastic work: stress response of a polycrystalline aggregate on prescribed loading ratios

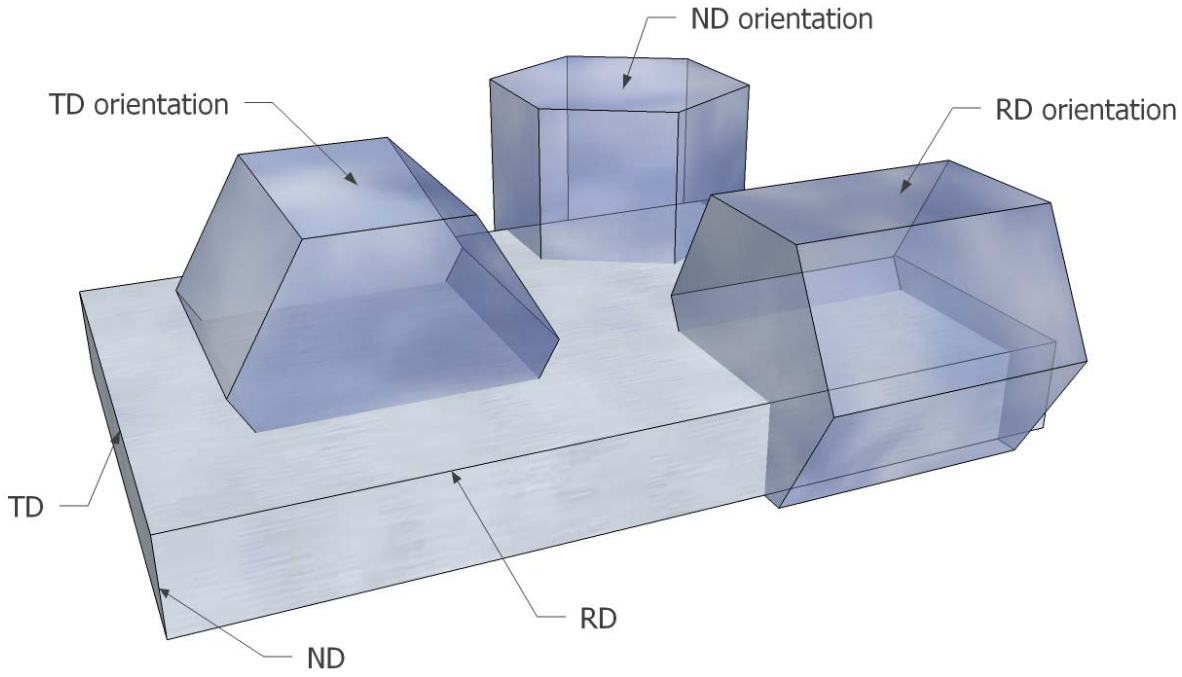

Figure 5: Three basic orientations of the single crystal with respect to the orthogonal system; RD, TD and ND are rolling, transverse and normal direction of the rolled sheet, respectively

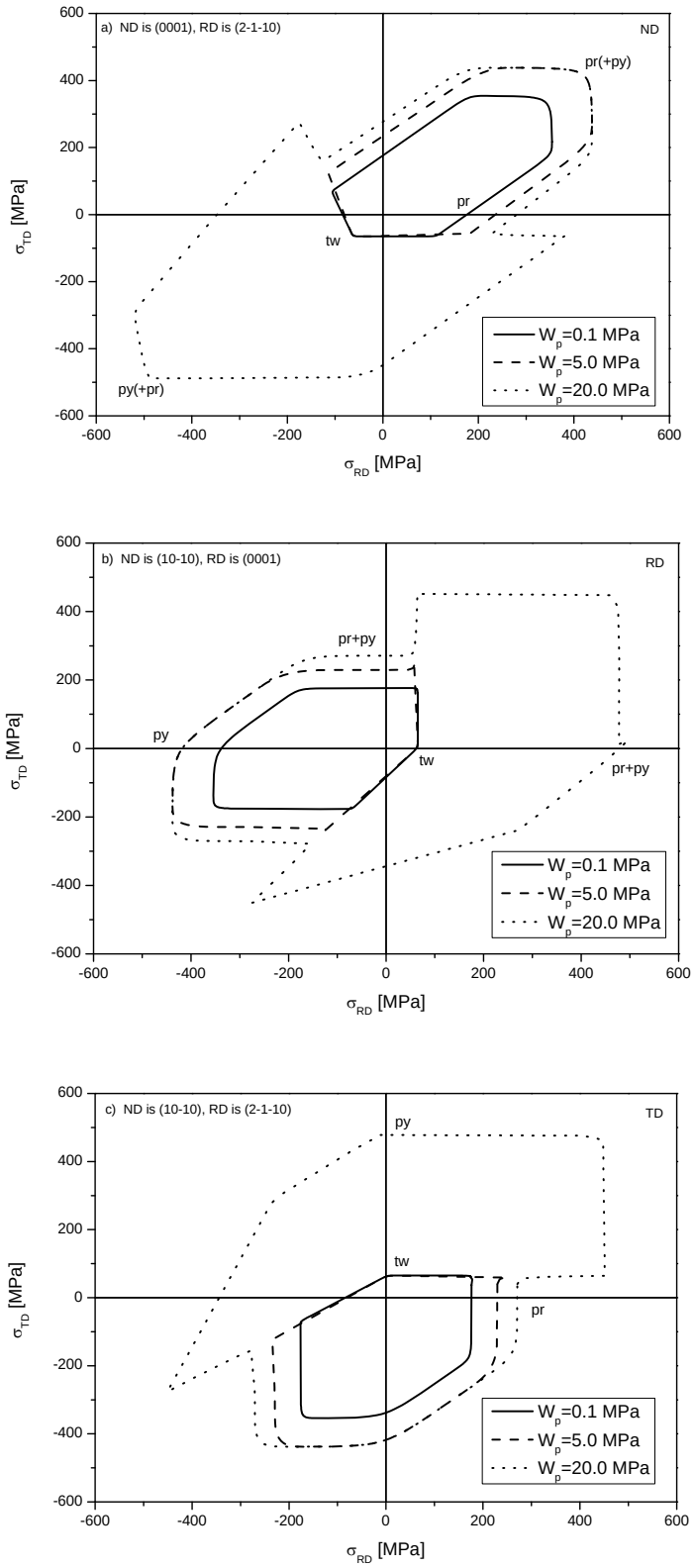

Figure 6: Contours of plastic work obtained from biaxial in-plane probing on a single crystal: ND-orientation (a), RD-orientation (b) and TD-orientation (c)

a)

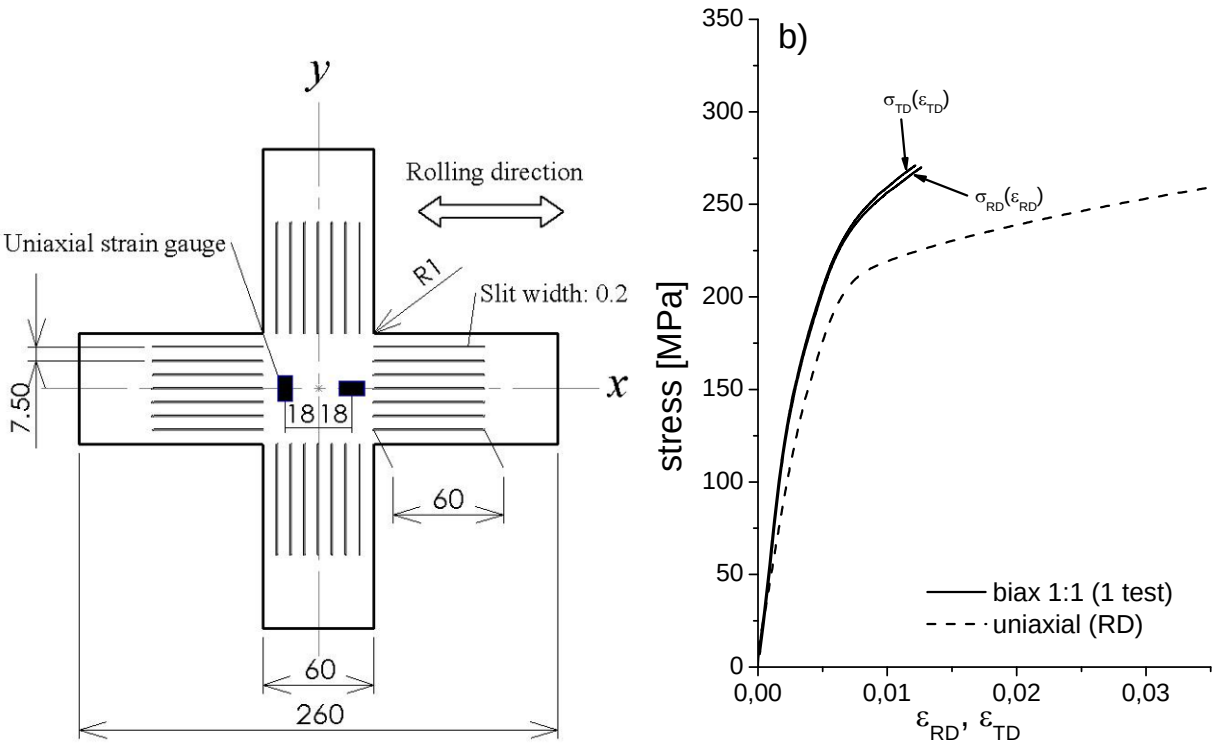

Figure 7: Geometry of cruciform specimen, dimensions in mm (a) and results of the biaxial test obtained from a cruciform specimen conducted under loading ratio 1:1 (b)

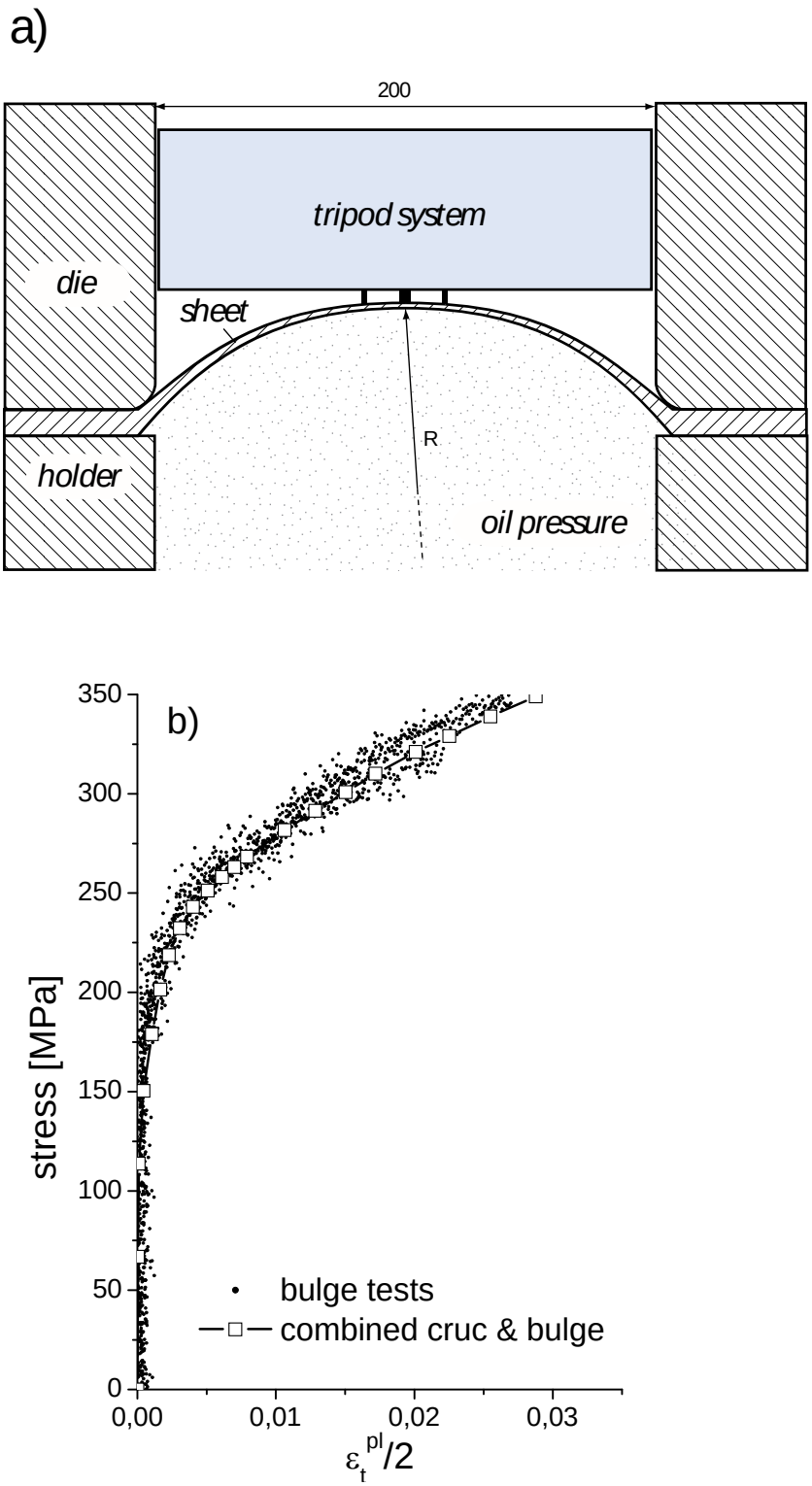

Figure 8: Bulge test setup (a) and stress-plastic strain response from the hydraulic bulge test (b). The symbols represent a combination of cruciform specimen test and bulge test results

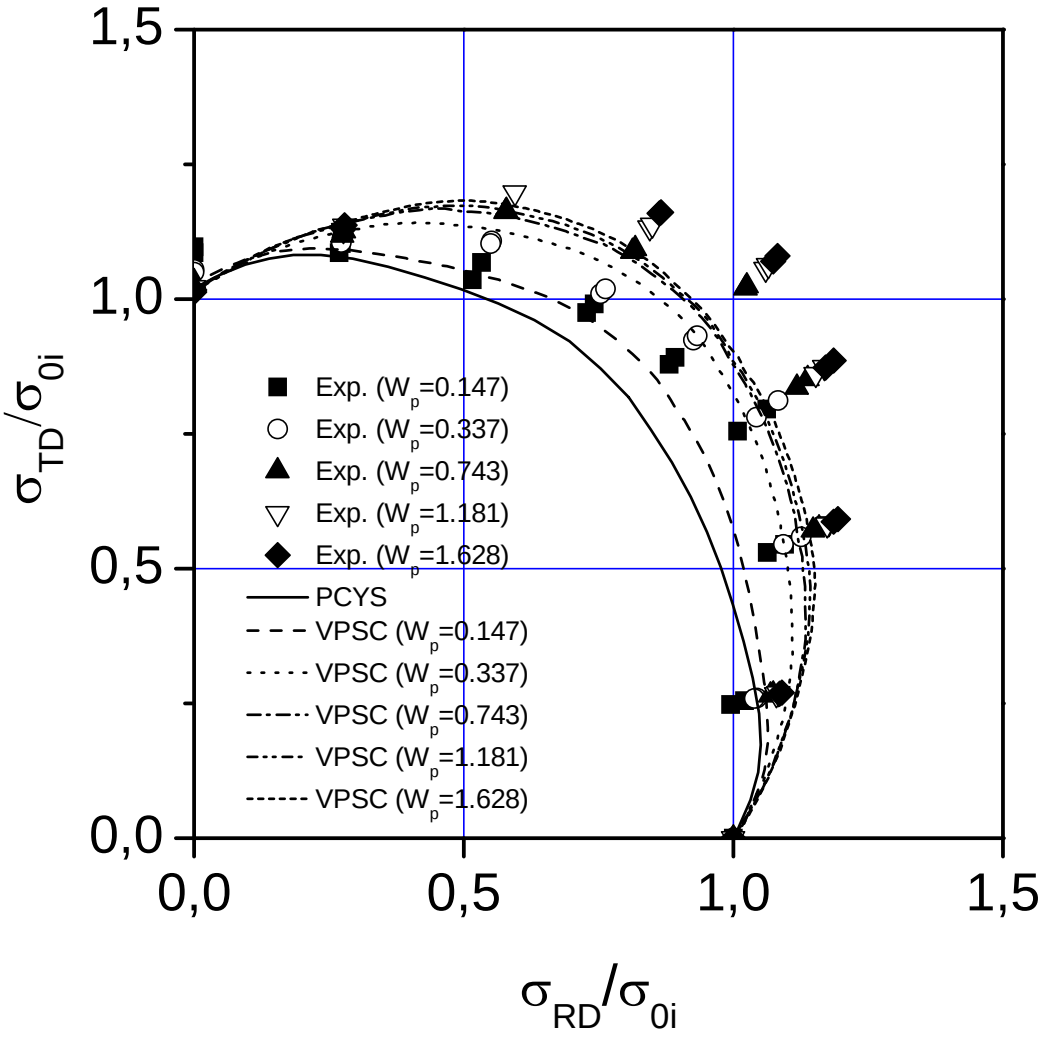

Figure 9: Iso-work contours obtained by biaxial testing [19] (symbols) and the respective predictions of the VPSC model (lines). Stresses have been normalised by the respective uniaxial stress σ_0 in RD. The plastic work levels correspond to plastic strains in RD tension of 0.001, 0.002, 0.004, 0.006 and 0.008.

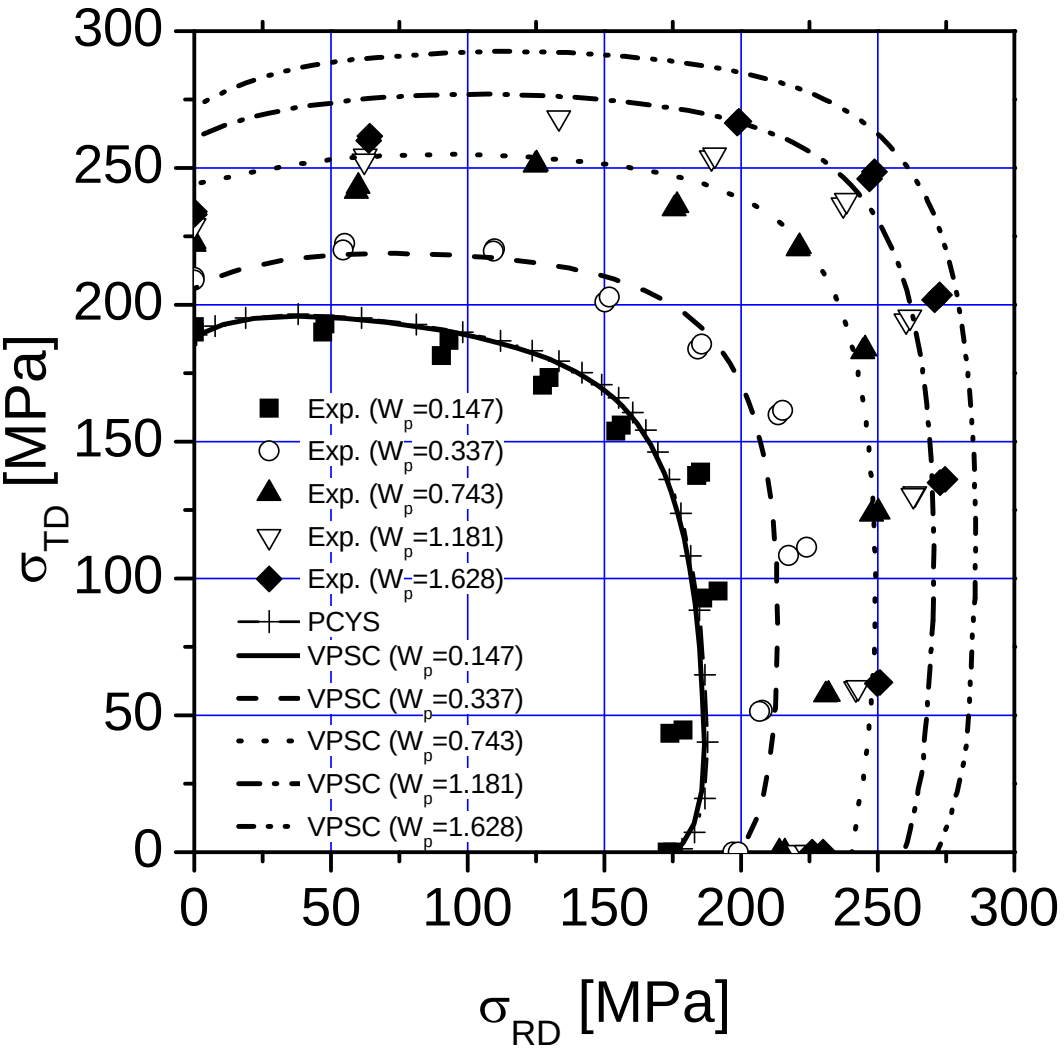

Figure 10: Iso-work contours obtained by biaxial testing [19] (symbols) and the respective predictions of the VPSC model (lines) using updated parameters. The plastic work levels correspond to plastic strains in RD tension of 0.001, 0.002, 0.004, 0.006 and 0.008.

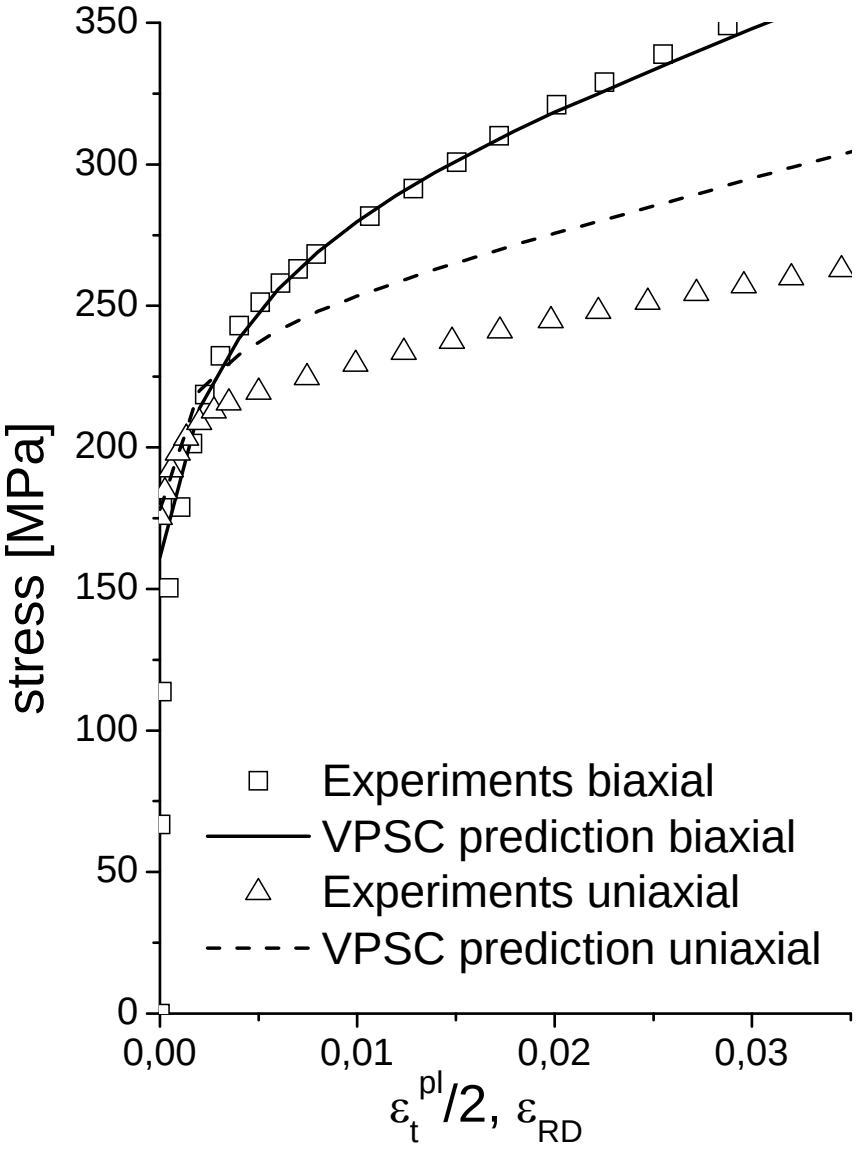

Figure 11: experimental and numerical response for uniaxial and biaxial loadings (uniaxial data cropped)

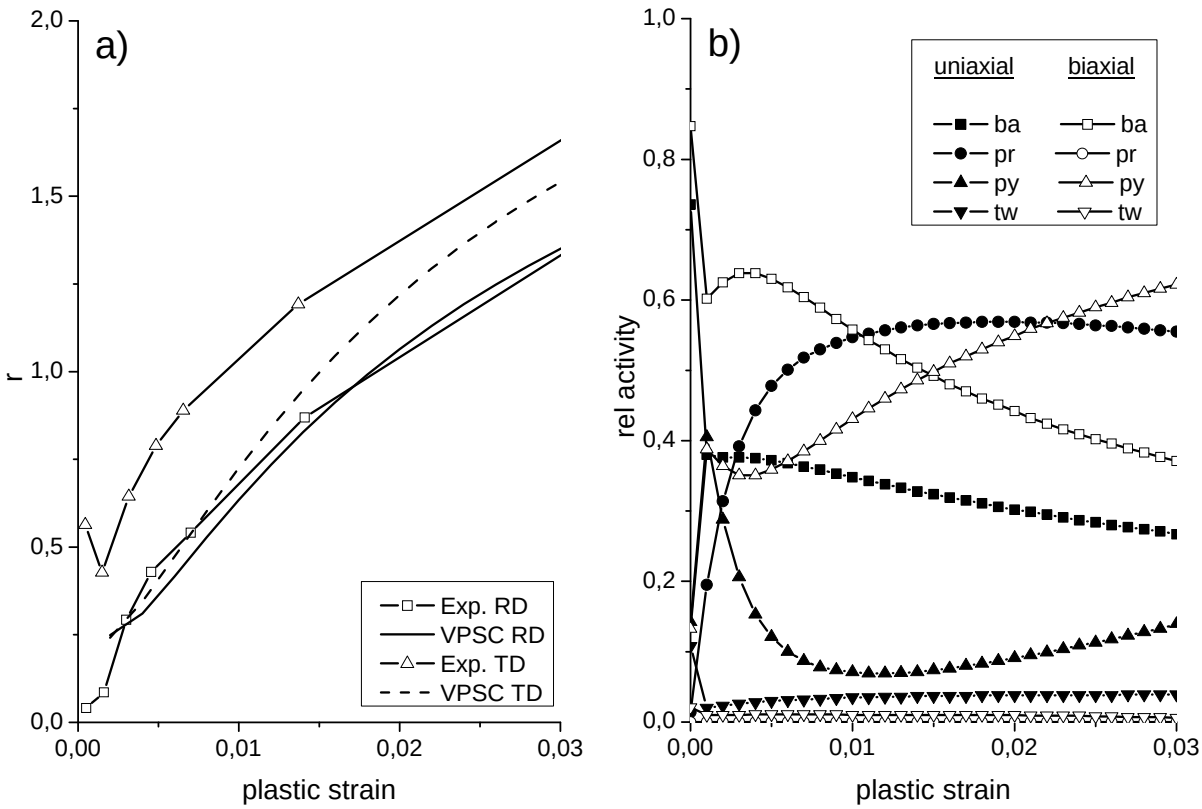

Figure 12: evolution of the r-value (experiments taken from [19]) (a) and relative activities of slip systems in case of uniaxial tension (RD) and biaxial tension (VPSC results) (b)